OXFORD JOURNAL
OF STUDENT
SCHOLARSHIP

Multi-Target Virtual Screening of Phytochemicals Against Key Molecular Targets in Ovarian Cancer: An Integrated Molecular Docking, Pharmacokinetic, and Toxicity Analysis

Kashvi Goel
goelkashvi01@gmail.com

ABSTRACT

Most ovarian cancers are diagnosed at an advanced stage and eventually become resistant to platinum- and taxane-based chemotherapy. Single-target agents such as PARP inhibitors benefit only genomically defined subgroups, which has motivated interest in compounds able to engage several oncogenic nodes at once. This study asked whether an ethnopharmacologically curated phytochemical library contains compounds predicted to bind multiple ovarian cancer-associated proteins while also carrying acceptable predicted drug-like properties. Forty-five phytochemicals from Dr. Duke's Phytochemical and Ethnobotanical Database, together with etoposide as a comparator, were docked with AutoDock Vina against five proteins: VEGFA (1FLT), Bcl-xL (3ZLN), MCL-1 (4WMR), PARP-1 (5DS3), and STAT3 (6NJS). Docking was followed by SwissADME pharmacokinetic profiling, ProTox-II toxicity prediction, and residue-level interaction analysis. The 230 protein–ligand calculations returned predicted binding affinities from −14.6 to −3.6 kcal mol^{-1}. Applying an operational screening threshold of $\Delta G \leq -7.0$ kcal mol^{-1}, three phytochemicals elemene, γ-tocopherol, and ursolic acid met the threshold against all five targets, while α-carotene, berberine, and berberastine met it against four of five with more favourable predicted drug-likeness. Across the phytochemical library, 34 of 45 compounds (75.6%) showed no Lipinski Rule-of-Five violations, but the strongest binders, elemene and γ-tocopherol, were predicted to have low gastrointestinal absorption. Interaction analysis showed that elemene engaged all five proteins exclusively through hydrophobic and alkyl contacts, whereas etoposide and γ-tocopherol also formed hydrogen bonds and π–π stacking contacts at sub-pockets including the PARP-1 catalytic loop and the Bcl-xL BH3-binding groove. Because docking scores correlated strongly with molecular weight, apparent multi-target performance may partly reflect ligand size rather than specific recognition. These results are therefore hypothesis-generating: elemene, α-carotene, and the berberine/berberastine scaffold are prioritised for experimental binding and functional testing, and no claim of therapeutic activity is made on computational grounds alone.

Keywords: ovarian cancer; molecular docking; multi-target virtual screening; phytochemicals; AutoDock Vina; pharmacokinetics; ADMET; SwissADME; ProTox-II; polypharmacology

INTRODUCTION

Ovarian cancer remains one of the most lethal malignancies affecting women worldwide. GLOBOCAN 2022 recorded 324,603 new cases and 206,956 deaths globally (Ferlay et al., 2024; Sung et al., 2021). More than two-thirds of cases are detected at Stage III or IV, once disease has spread beyond the pelvis, and five-year survival falls to roughly 30–40% for Stage III and 15–20% for Stage IV disease. Late detection, rather than incidence alone, is the principal driver of this mortality.

Approximately 90% of epithelial ovarian cancers are managed with cytoreductive surgery followed by platinum- and taxane-based chemotherapy, most commonly carboplatin with paclitaxel (Armstrong et al., 2006). Initial response rates are high, but most patients relapse, and repeated platinum exposure carries cumulative toxicity and hypersensitivity risk. The anti-angiogenic antibody bevacizumab has activity in combination regimens (Burger et al., 2011), and PARP inhibitors such as olaparib and niraparib improve progression-free survival (Moore et al., 2018). Neither class, however, has substantially changed outcomes in platinum-resistant or recurrent disease across unselected patients: PARP inhibitor benefit remains largely confined to homologous-recombination-deficient subgroups, and overall-survival data contributed to the withdrawal of approval for PARP inhibitor monotherapy in recurrent disease (Goldlust et al., 2024). Single-target agents are also vulnerable to compensatory pathway activation, which has prompted interest in compounds that engage several nodes of an oncogenic network simultaneously (Anighoro et al., 2014).

Five proteins with distinct, well-characterised roles in ovarian cancer biology were therefore selected as a target panel. VEGFA drives tumour angiogenesis and is associated with peritoneal dissemination and poor prognosis. The pro-survival BCL-2 family members Bcl-xL and MCL-1 permit evasion of apoptosis under therapeutic stress, a mechanism particularly associated with platinum resistance (Czabotar et al., 2014). PARP-1 is central to the DNA damage response and underlies synthetic lethality in BRCA-deficient cells (Ashworth & Lord, 2018). STAT3, activated constitutively by cytokines such as IL-6, supports survival, immune evasion, and cancer stem cell maintenance, and its activation is linked to chemoresistance (Johnson et al., 2018). Together these targets span angiogenesis, apoptosis evasion, DNA repair, and transcriptional oncogenesis.

Natural products remain a productive source of anticancer pharmacophores: approximately 65% of small-molecule anticancer drugs approved between 1981 and 2019 were natural products, their semisynthetic derivatives, or natural-product mimetics (Newman & Cragg, 2020). Paclitaxel, vincristine, camptothecin, and etoposide all derive from plant metabolites. Phytochemicals are attractive starting points for multi-target discovery because of their structural diversity and intrinsic polypharmacology. Candidate compounds for this study were drawn from Dr. Duke's Phytochemical and Ethnobotanical Databases (Duke, n.d.), with three-dimensional structures retrieved from PubChem (Kim, S., et al., 2023). Structure-based virtual screening by molecular docking allows such libraries to be prioritised rapidly, and AutoDock Vina was used here for its validated scoring function and computational efficiency (Trott & Olson, 2010). Because inadequate pharmacokinetics, rather than absent target engagement, accounts for a

large share of candidate attrition, docking was paired with SwissADME physicochemical and absorption profiling (Daina et al., 2017) and ProTox-II toxicity prediction (Banerjee et al., 2018).

Molecular docking has been applied to individual ovarian cancer targets, and individual phytochemicals have been screened against specific oncoproteins in other tumour types. We are not aware of a published study that combines multi-target docking of an ethnopharmacologically curated phytochemical library against this particular five-protein panel with pharmacokinetic and toxicity filtering in a single workflow, although our literature search was not systematic and we do not claim that no such study exists. The research question addressed here is therefore specific and comparative rather than one of priority: among 45 phytochemicals screened under identical docking conditions, which compounds show favourable predicted binding across several mechanistically distinct ovarian cancer-associated proteins, and do those compounds also carry predicted pharmacokinetic and toxicity profiles compatible with further development? The aim is to generate a ranked, experimentally testable shortlist, not to establish inhibitory activity.

MATERIALS AND METHODS

Study Design and Computational Workflow

A structure-based multi-target virtual screening strategy was used to evaluate the predicted binding of selected phytochemicals against five proteins implicated in ovarian cancer-associated signalling, survival, angiogenesis, and DNA-damage responses. The workflow comprised target retrieval and preparation, ligand preparation, molecular docking, ranking of protein–ligand complexes by predicted binding affinity, residue-level interaction analysis, and in silico assessment of pharmacokinetic and toxicity properties. Comparable multi-target computational strategies have previously been used to prioritise phytochemicals against cancer-associated proteins (Jha et al., 2022a, 2022b).

The docking panel comprised vascular endothelial growth factor A (VEGFA; PDB ID 1FLT), B-cell lymphoma-extra large (Bcl-xL; PDB ID 3ZLN), myeloid cell leukemia-1 (MCL-1; PDB ID 4WMR), poly(ADP-ribose) polymerase-1 (PARP-1; PDB ID 5DS3), and signal transducer and activator of transcription 3 (STAT3; PDB ID 6NJS). Etoposide was included as a comparator compound to provide a common reference point across the panel; its role and limitations are defined in the Comparator Compound subsection below.

Retrieval and Preparation of Target Proteins

Three-dimensional structures of the five targets were obtained from the Protein Data Bank using the identifiers 1FLT, 3ZLN, 4WMR, 5DS3, and 6NJS. Structures were prepared before docking to remove components not required for receptor–ligand calculation, and were converted to the PDBQT format required by AutoDock Vina. This preparation strategy follows previously reported multi-target docking

workflows (Jha et al., 2022a, 2022b). The prepared receptor files were designated 1FLT_Processed.pdbqt, 3ZLN_Processed.pdbqt, 4WMR_Processed.pdbqt, 5DS3_Processed.pdbqt, and 6NJS_Processed.pdbqt.

Phytochemical Library and Ligand Preparation

The ligand library comprised 45 phytochemicals. Three-dimensional structures were obtained from PubChem and prepared using a standardised ligand-preparation workflow, then converted to PDBQT format, which supplies the atom-type, charge, and torsional information required by AutoDock Vina. Etoposide was processed by the same procedure, so that differences in input structure handling would not contribute to score differences between the comparator and the library. The use of PubChem-derived structures converted to docking-compatible formats follows established phytochemical virtual-screening practice (Jha et al., 2022a, 2022b).

Where a database entry corresponds to a class of related structures rather than a single defined molecule as for the entries recorded here as ginsenosides and anthocyanins a single representative structure was docked, and results for those entries should be read as applying to that representative structure only. Likewise, the ligand docked as elemene is the parent sesquiterpene structure retrieved from PubChem; it is not stereochemically identical to the β-elemene isomer used in the experimental literature cited in the Discussion, and the two are distinguished explicitly throughout.

Molecular Docking

Docking was performed with AutoDock Vina using a rigid-receptor, flexible-ligand protocol to predict preferred binding poses and corresponding predicted binding affinities. The search space was defined independently for each receptor to ensure adequate coverage of the region sampled, and the exhaustiveness parameter was set to 8 for all calculations, maintaining identical search intensity across the five targets. Scores are reported as predicted binding affinities in kcal mol^{-1}, with more negative values indicating more favourable predicted binding. Grid-box centres and dimensions are given in Table 1.

Table 1. AutoDock Vina grid-box parameters for the five target proteins. Exh. = exhaustiveness.

Target	PDB ID	Center X	Center Y	Center Z	Size X (Å)	Size Y (Å)	Size Z (Å)	Exh.
VEGFA	1FLT	1.8117	6.5101	19.2819	52.0352	45.9037	39.4785	8
Bcl-xL	3ZLN	−24.9153	−3.5150	15.9151	40.3535	37.9675	36.5579	8
MCL-1	4WMR	−14.4923	−13.9294	12.3264	40.5727	43.5331	40.0892	8
PARP-1	5DS3	5.5047	37.1051	10.2222	50.5283	52.7787	41.1950	8

Target	PDB ID	Center X	Center Y	Center Z	Size X (Å)	Size Y (Å)	Size Z (Å)	Exh.
STAT3	6NJS	−2.4849	19.2647	24.6206	78.4305	115.8948	88.4458	8

Receptor-specific rather than standardised search spaces were used to accommodate differences in protein size and in the spatial distribution of the sampled regions. Target-specific grid definitions have similarly been used in previous AutoDock Vina-based multi-target phytochemical screens (Jha et al., 2022a, 2022b). The grid boxes used here are large relative to a single binding site, so the calculations are best described as blind or near-blind docking across an extended surface rather than as docking into a pre-validated orthosteric pocket.

Definition of a Hit and Justification of the Docking Threshold

For each protein–ligand pair, the pose with the most favourable predicted binding affinity was retained. A compound was operationally defined as a hit against a given target when its best predicted binding affinity met the threshold $\Delta G \leq -7.0$ kcal mol^{-1}. This definition is applied consistently throughout the manuscript, and the same inequality is used in the Abstract, Results, tables, and Discussion.

Three points about this threshold should be stated explicitly. First, −7.0 kcal mol^{-1} is a pragmatic screening heuristic in common use for prioritising docking output; it is not a validated activity cut-off, and it does not correspond to any measured affinity. A compound meeting it has not been shown to bind or inhibit its target. Second, the value was chosen before compound ranking and applied uniformly to all five targets rather than tuned per target, but it was not calibrated against known actives, and no decoy set, re-docking of co-crystallised ligands, or enrichment analysis was performed to establish that the scoring function discriminates binders from non-binders on this panel. The threshold is therefore a descriptive filter, not a validated classifier. Third, the threshold sits within the body of the score distribution rather than at an extreme: mean predicted affinities ranged from −5.82 kcal mol^{-1} for VEGFA to −7.88 kcal mol^{-1} for Bcl-xL, so the number of compounds classified as hits is sensitive to small changes in the cut-off. For this reason, full score matrices are reported for every compound and target, and the continuous rank order of predicted affinities, rather than threshold membership alone, is treated as the primary result.

A multi-target coverage score from zero to five was obtained by counting the targets meeting this threshold for each compound. Compounds meeting it for all five proteins are described as five-target hits and those meeting it for four as broad multi-target candidates. This counting distinguishes compounds with a single exceptional score from those with consistent predicted affinities across the panel; it is not a measure of potency.

Comparator Compound

Etoposide was included as a comparator rather than as a positive control, and the distinction is material to interpretation. Etoposide is a semisynthetic derivative of the plant lignan podophyllotoxin and acts clinically as a topoisomerase II poison. Topoisomerase II is not a member of the present target panel, and etoposide is not an established ligand of VEGFA, Bcl-xL, MCL-1, PARP-1, or STAT3. Its docking scores therefore cannot validate the docking protocol, cannot be read as a benchmark of true binding, and do not indicate that compounds scoring near it share its mechanism. Etoposide serves only to place the phytochemical scores on a common numerical scale against a clinically used, plant-derived anticancer agent of comparable or greater molecular size. Its high scores should be interpreted alongside the molecular weight dependence of the scoring function reported in the Results.

Protein-Ligand Interaction Analysis

Residue-level interaction analysis was applied to the top-ranked complexes, and two-dimensional protein–ligand interaction diagrams were generated for the prioritised phytochemicals and the comparator compound. Conventional hydrogen bonds, carbon–hydrogen bonds, van der Waals contacts, alkyl and π-alkyl interactions, π–π stacking, π–π T-shaped interactions, and π-sulfur contacts were recorded, as were unfavourable contacts such as donor–donor interactions where present. Similar interaction-based characterisation has been used to add residue-level detail to docking scores (Jha et al., 2022a). Elemene, γ-tocopherol, and etoposide were analysed against all five proteins, producing fifteen interaction maps.

In Silico Pharmacokinetic and Drug-Likeness Assessment

Physicochemical and pharmacokinetic properties were evaluated with SwissADME using canonical SMILES as input. Molecular weight, consensus Log P, predicted gastrointestinal (GI) absorption, blood–brain barrier permeability, aqueous solubility, and bioavailability-related parameters were recorded. Drug-likeness was assessed by Lipinski's Rule of Five, with the number of violations recorded for each compound rather than treating Rule-of-Five compliance as an absolute measure of suitability. SwissADME profiling has been incorporated into comparable multi-target phytochemical screening pipelines (Jha et al., 2022a, 2022b).

Computational Toxicity Prediction

Potential toxicity was assessed in silico with ProTox-II using canonical SMILES input, recording the predicted median lethal dose (LD50, mg kg^{-1}) and acute oral toxicity class. ProTox-II assigns compounds to six classes, with lower class numbers indicating greater predicted acute toxicity. Toxicity predictions were used alongside docking and pharmacokinetic parameters as a secondary prioritisation criterion, not as an independent determination that a compound is safe or unsafe (Jha et al., 2022a).

Integrated Candidate Prioritisation

Candidates were selected on an integrated assessment rather than docking affinity alone. For each phytochemical, predicted target coverage was considered together with its strongest docking score, SwissADME physicochemical and pharmacokinetic properties, Rule-of-Five violations, predicted GI absorption, bioavailability, and ProTox-II estimates. Priority was given to compounds combining favourable predicted binding across several proteins with acceptable predicted pharmacokinetic and toxicological characteristics.

Statistical Analysis

Descriptive statistics were used to summarise the distribution of predicted binding affinities across the five targets, and mean docking affinities were computed per receptor across the screened library. Pearson correlation analysis was used to test whether the strongest predicted affinity per compound was associated with molecular descriptors, specifically molecular weight and consensus Log P. Statistical significance was assessed at $P < 0.05$, and results were interpreted from the direction and magnitude of the correlation coefficient (r), with negative coefficients indicating that higher descriptor values were associated with more negative docking scores. Docking affinities were also displayed as a heatmap to compare compound- and target-specific patterns.

RESULTS

Multi-Target Docking Across the Five-Protein Panel

The screening library comprised 45 phytochemicals with three-dimensional structures retrieved from PubChem, together with etoposide as the comparator compound. Each compound was docked against VEGFA (1FLT), Bcl-xL (3ZLN), MCL-1 (4WMR), PARP-1 (5DS3), and STAT3 (6NJS), giving 230 protein–ligand docking calculations in total, of which 225 involved the phytochemical library. Predicted binding affinities across the dataset ranged from −14.6 to −3.6 kcal mol^{-1}. These values are scoring-function outputs and are not measured binding free energies.

Bcl-xL and PARP-1 showed the most favourable overall ligand-binding profiles, with mean predicted affinities of −7.88 and −7.86 kcal mol^{-1} respectively. MCL-1 was intermediate at −7.34 kcal mol^{-1} and STAT3 averaged −6.44 kcal mol^{-1}, while VEGFA showed the least favourable mean value at −5.82 kcal mol^{-1}. Etoposide returned predicted affinities from −8.9 to −14.6 kcal mol^{-1} across the panel.

Ranking the 45 phytochemicals by strongest single-target affinity showed clear separation among the leading compounds (Table 2; Figure 1). γ-Tocopherol was the strongest phytochemical binder, at −12.5 kcal mol^{-1} against Bcl-xL, followed by α-carotene (−10.9 kcal mol^{-1}, Bcl-xL), β-carotene (−10.7 kcal mol^{-1}, Bcl-xL), and elemene (−10.4 kcal mol^{-1}, Bcl-xL). Bcl-xL was also the most frequently preferred target among top-ranked compounds, returning the best score for eight of the top 15.

Figure 1. Predicted binding affinities (kcal mol^{-1}) for the top 20 phytochemicals across the five-protein panel. Rows are ordered by strongest single-target affinity; darker green indicates more negative predicted binding.

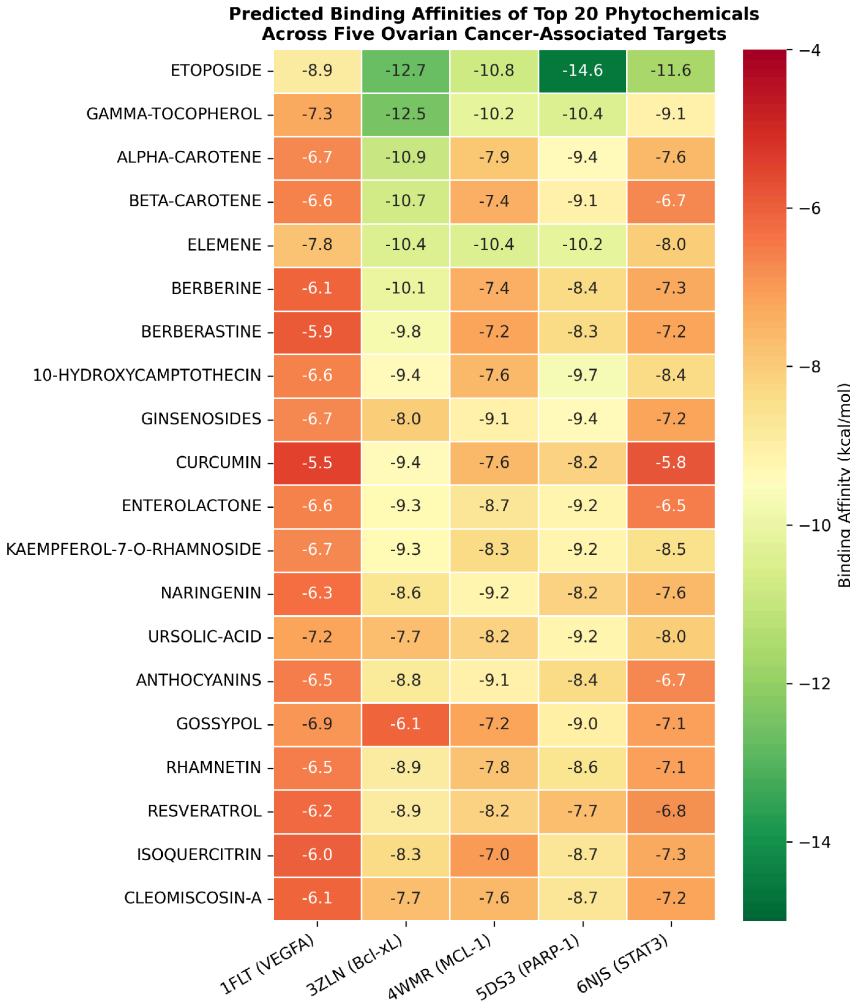


Table 2. Top 15 compounds ranked by strongest predicted binding affinity (ΔG, kcal mol^{-1}). "Targets ≤ −7.0" gives the number of targets meeting the operational threshold. *Comparator compound. †Entry represents a compound class; a single representative structure was docked.

Rank	Compound	1FLT (VEGFA)	3ZLN (Bcl-xL)	4WMR (MCL-1)	5DS3 (PARP-1)	6NJS (STAT3)	Best ΔG	Targets ≤ −7.0
1	Etoposide*	−8.9	−12.7	−10.8	−14.6	−11.6	−14.6	5/5
2	γ-Tocopherol	−7.3	−12.5	−10.2	−10.4	−9.1	−12.5	5/5
3	α-Carotene	−6.7	−10.9	−7.9	−9.4	−7.6	−10.9	4/5
4	β-Carotene	−6.6	−10.7	−7.4	−9.1	−6.7	−10.7	3/5
5	Elemene	−7.8	−10.4	−10.4	−10.2	−8.0	−10.4	5/5
6	Berberine	−6.1	−10.1	−7.4	−8.4	−7.3	−10.1	4/5
7	Berberastine	−5.9	−9.8	−7.2	−8.3	−7.2	−9.8	4/5
8	10-Hydroxycamptothecin	−6.6	−9.4	−7.6	−9.7	−8.4	−9.7	4/5
9	Ginsenosides†	−6.7	−8.0	−9.1	−9.4	−7.2	−9.4	4/5
10	Curcumin	−5.5	−9.4	−7.6	−8.2	−5.8	−9.4	3/5
11	Enterolactone	−6.6	−9.3	−8.7	−9.2	−6.5	−9.3	3/5
12	Kaempferol-7-O-rhamnoside	−6.7	−9.3	−8.3	−9.2	−8.5	−9.3	4/5
13	Naringenin	−6.3	−8.6	−9.2	−8.2	−7.6	−9.2	4/5
14	Ursolic acid	−7.2	−7.7	−8.2	−9.2	−8.0	−9.2	5/5
15	Anthocyanins†	−6.5	−8.8	−9.1	−8.4	−6.7	−9.1	3/5

Phytochemicals Meeting the Threshold Against All Five Targets

Applying the operational threshold ΔG ≤ −7.0 kcal mol^{-1} across the panel, three phytochemicals γ-tocopherol, elemene, and ursolic acid met the threshold for all five targets, as did the etoposide comparator (Table 2). A further seven compounds α-carotene, berberine, berberastine,

10-hydroxycamptothecin, ginsenosides, kaempferol-7-O-rhamnoside, and naringenin met it for four of five proteins. β-Carotene, curcumin, enterolactone, and anthocyanins met it for three. Several compounds therefore achieved strong individual docking scores while only a smaller subset maintained favourable predicted affinities across most or all of the panel. As noted in the Methods, membership of these categories is sensitive to the chosen cut-off and should be read together with the continuous scores in Table 2.

Target-Wise Trends and the Molecular Weight Confound

Target-specific analysis further distinguished the binding patterns of the leading compounds (Table 2; Supplementary Table S1). γ-Tocopherol and elemene were among the strongest binders across multiple targets, consistent with their five-target profiles. After the etoposide comparator, 10-hydroxycamptothecin was among the strongest phytochemical ligands for PARP-1, at −9.7 kcal mol^{-1}.

Differences among flavonoids and related compounds were also apparent. Naringenin showed its strongest predicted interaction with MCL-1 (−9.2 kcal mol^{-1}), kaempferol-7-O-rhamnoside returned −8.5 kcal mol^{-1} against STAT3, and anthocyanins returned −9.1 kcal mol^{-1} against MCL-1. These compounds generally returned less favourable predicted affinities toward VEGFA, indicating substantial target-dependent variation within the screened chemical space.

Across the full 45-compound dataset, the strongest target-specific docking affinity correlated strongly with molecular weight (Pearson $r = -0.74$, $P < 0.001$), and more weakly with consensus Log P ($r = -0.44$, $P = 0.003$). Larger and, to a lesser extent, more lipophilic molecules therefore tended to return more negative best-target docking scores. This is a well-recognised property of empirical scoring functions and is an important qualification on the rankings reported here: a substantial part of the variance in best-target score is explained by size alone. Several of the top-ranked compounds, including etoposide (588.56 g mol^{-1}), α- and β-carotene (536.87 g mol^{-1}), and ursolic acid (456.70 g mol^{-1}), are among the largest in the library, so their positions in the ranking cannot be attributed to specific molecular recognition without further evidence. Elemene (204.35 g mol^{-1}) is a notable exception, since it met the threshold against all five targets despite being one of the smallest compounds screened.

Pharmacokinetic Profiling

Among the 45 phytochemicals, 34 (75.6%) showed no Lipinski Rule-of-Five violations, seven had one violation, and four had two or more (Table 3; Supplementary Table S2). High predicted GI absorption was recorded for 34 compounds, and 21 (46.7%) were predicted to cross the blood–brain barrier.

The multi-target candidates showed distinct profiles. α-Carotene and β-carotene had no Lipinski violations, high predicted GI absorption, and bioavailability scores of 0.55. Berberine and berberastine likewise showed no violations and high predicted GI absorption alongside their four-target profiles. By contrast, γ-tocopherol and ginsenosides had less favourable predicted absorption, both classified as poorly soluble by the ESOL model with low predicted GI absorption and consensus Log P values of 7.83 and

6.75 respectively. Elemene was also predicted to have low GI absorption despite its five-target profile. Ursolic acid had the highest bioavailability score among the leads in Table 3 at 0.85, although its predicted GI absorption was also low.

Table 3. Predicted pharmacokinetic and toxicity properties of selected leading compounds (SwissADME, ProTox-II). *Comparator compound. †Entry represents a compound class. n/a: no ProTox-II value available.

Compound	MW (g/mol)	Lipinski viol.	Log P (cons.)	GI absorp.	BBB perm.	Bioavail. score	LD50 (mg/kg)	Toxicity class
Etoposide*	588.56	2	1.17	Low	No	0.17	215	3
γ-Tocopherol	416.68	1	7.83	Low	No	0.55	5000	5
α-Carotene	536.87	0	2.38	High	Yes	0.55	1510	4
β-Carotene	536.87	0	2.53	High	Yes	0.55	1510	4
Elemene	204.35	1	4.49	Low	No	0.55	5300	5
Berberine	336.36	0	2.53	High	Yes	0.55	200	3
Berberastine	352.36	0	1.72	High	Yes	0.55	200	3
10-Hydroxycamptothecin	364.35	0	1.83	High	No	0.55	50	3
Ginsenosides†	444.73	1	6.75	Low	No	0.55	2260	5
Curcumin	368.38	0	3.03	High	No	0.55	2000	4
Ursolic acid	456.70	1	5.93	Low	No	0.85	n/a	n/a

Predicted Toxicity Profiles

ProTox-II predictions spanned toxicity classes 2 to 6, with higher class numbers indicating lower predicted acute toxicity. No compound was assigned to Class 1 and one compound was assigned to Class 2. Class 4 (n = 15) and Class 5 (n = 12) were the most common assignments, three compounds were assigned to Class 6, and the remainder were assigned to Class 3.

Elemene was assigned to Class 5 with a predicted LD50 of 5300 mg kg^{-1}, and γ-tocopherol to Class 5 with a predicted LD50 of 5000 mg kg^{-1}. 10-Hydroxycamptothecin was assigned to Class 3 with a considerably lower predicted LD50 of 50 mg kg^{-1}, and berberine and berberastine were also assigned to

Class 3, each with a predicted LD50 of 200 mg kg^{-1}. These predictions separate the leading candidates by predicted acute toxicity as well as by docking performance.

Residue-Level Interaction Analysis

Fifteen two-dimensional interaction maps were generated for elemene, γ-tocopherol, and etoposide across all five targets (Figures 2–4; Table 4). The three ligands showed distinct interaction patterns.

Elemene, a small saturated sesquiterpene hydrocarbon without heteroatoms (TPSA = 0 $Å^2$), interacted with all five proteins exclusively through van der Waals and alkyl or π-alkyl contacts; no hydrogen bonds were identified at any of the five interfaces. Principal contacts were Val33, Leu54, Arg56, and Leu97 at VEGFA; Phe143, Phe144, Phe146, Met170, Leu174, and Cys151 at Bcl-xL; Ile182, Ile264, Leu267, Leu268, Leu298, Trp312, and Tyr185 at MCL-1; Leu920, Ile919, Phe897, His862, Ser864, and Leu877 at PARP-1; and Cys251, Ile258, Arg246, Pro256, Trp243, and Lys244 at STAT3.

Etoposide formed at least one conventional hydrogen bond at every target. At PARP-1 it formed a hydrogen bond with Gly863 and π–π stacking with Phe897, together with hydrophobic contacts involving Ala898, Leu921, and Val924, corresponding to the highest score in the dataset at −14.6 kcal mol^{-1}. At Bcl-xL it formed hydrogen bonds with Ala171 and Gly148 alongside contacts with Phe143, Phe144, Phe146, Ala142, and Val141, and it formed hydrogen bonds with Gln326 and Pro255 at STAT3 and with Leu186 at MCL-1.

γ-Tocopherol showed a third pattern, combining hydrophobic and aromatic contacts with target-dependent polar interactions. At Bcl-xL it contacted the Phe143/Phe144/Phe146 cluster and formed π–π stacked and T-shaped interactions with Trp188, corresponding to its strongest score of −12.5 kcal mol^{-1}. At MCL-1 it formed hydrophobic contacts with Leu210, Ile182, Ala291, and Val253, a hydrogen bond with Tyr185, and a π-sulfur interaction with Met199. At PARP-1 it engaged the Tyr896 and His862 region through π–π contacts and also contacted Phe897, Ile990, and Leu921, with one unfavourable donor–donor interaction involving Tyr907. Its STAT3 pose combined a hydrogen bond with Gln141 and contacts with Trp243, Cys251, and Leu337, but also contained multiple unfavourable contacts, making it the most sterically constrained of the five γ-tocopherol complexes. The presence of unfavourable contacts in two of the five poses indicates that these particular predictions should be treated with additional caution.

Figure 2. Two-dimensional interaction diagrams for elemene against (A) VEGFA (1FLT), (B) Bcl-xL (3ZLN), (C) MCL-1 (4WMR), (D) PARP-1 (5DS3), and (E) STAT3 (6NJS). Dashed lines denote non-covalent contacts; elemene engages all five proteins through van der Waals and alkyl/π-alkyl contacts only.

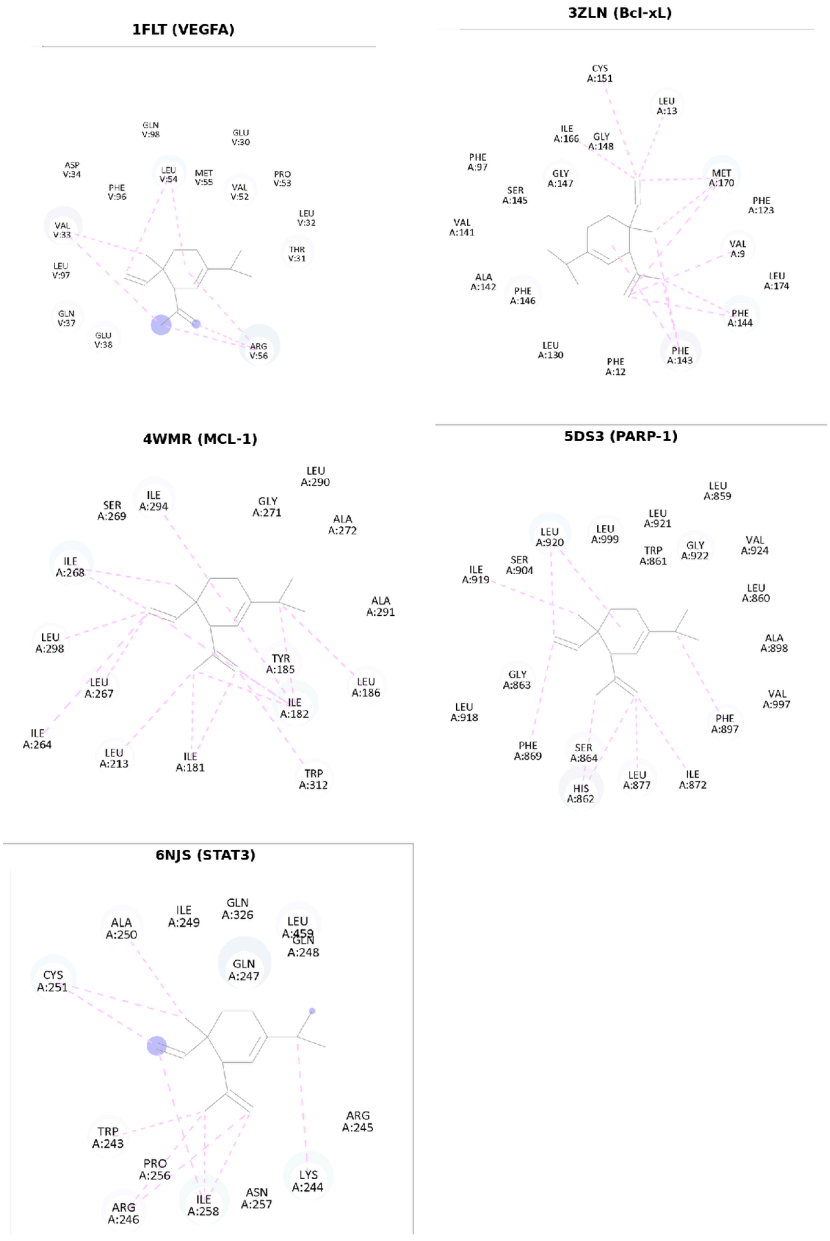
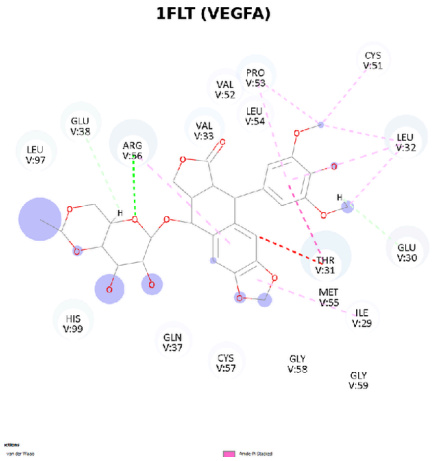
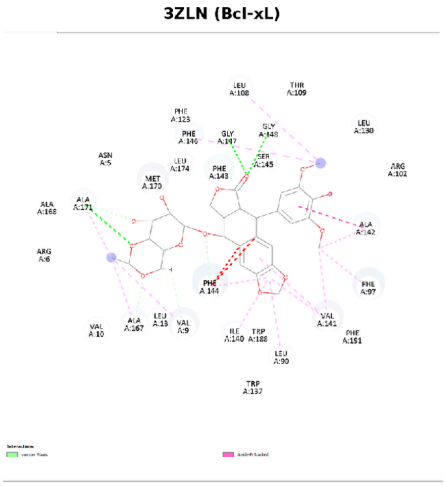
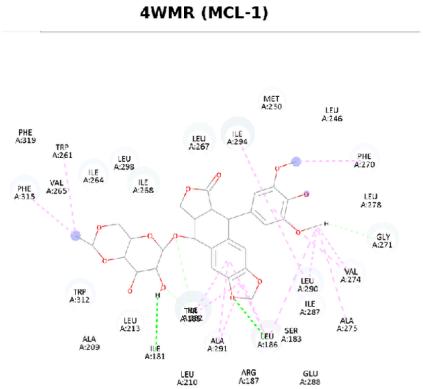
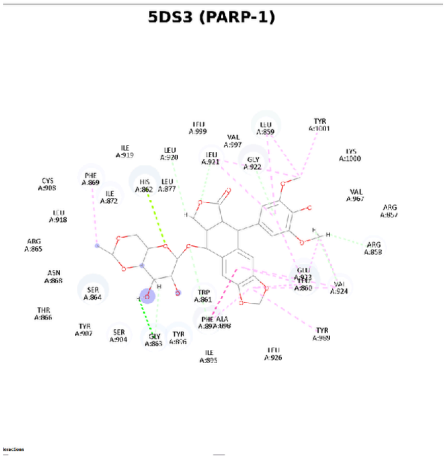


Figure 3. Two-dimensional interaction diagrams for the comparator compound etoposide against (A) VEGFA, (B) Bcl-xL, (C) MCL-1, (D) PARP-1, and (E) STAT3. Green dashed lines denote hydrogen bonds, pink lines alkyl, π-alkyl, π–π and amide–π contacts, and red lines unfavourable steric contacts.


1FLT (VEGFA)


3ZLN (Bcl-xL)


4WMR (MCL-1)


5DS3 (PARP-1)

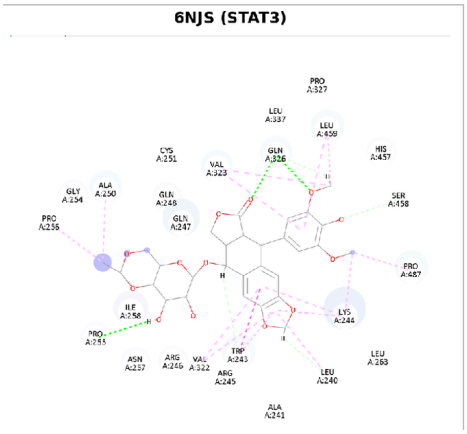

6NJS (STAT3)

Figure 4. Two-dimensional interaction diagrams for γ-tocopherol against (A) VEGFA, (B) Bcl-xL, (C) MCL-1, (D) PARP-1, and (E) STAT3. The Bcl-xL pose includes π–π stacked and T-shaped contacts with Trp188; the PARP-1 and STAT3 poses contain unfavourable contacts.

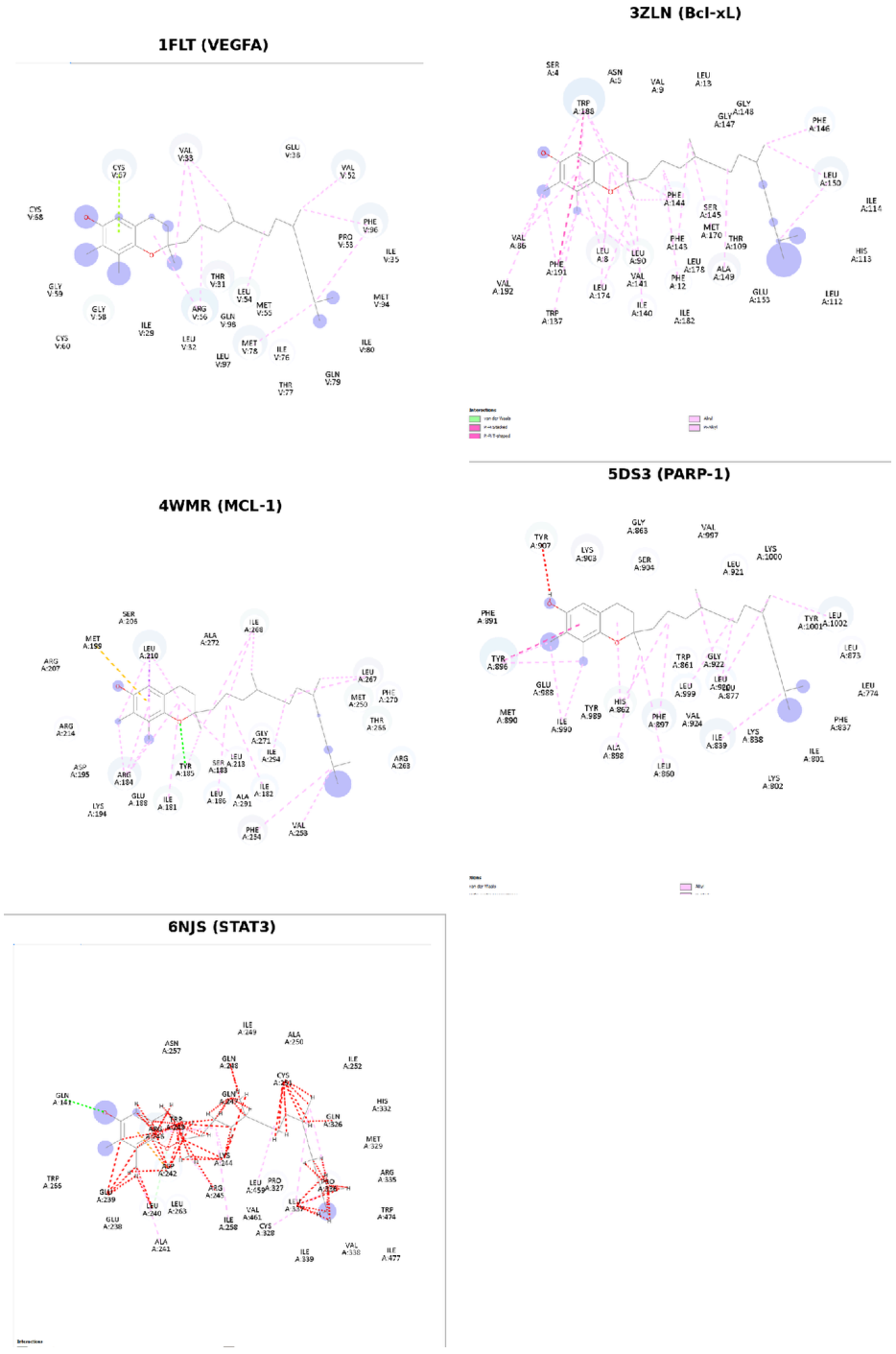

1FLT (VEGFA)
3ZLN (Bcl-xL)
4WMR (MCL-1)
5DS3 (PARP-1)
6NJS (STAT3)

Table 4. Key non-covalent interactions from the diagrams in Figures 2–4. *Comparator compound.

Compound	Target	Hydrogen bonds / special contacts	Dominant hydrophobic contacts	Interaction character
Elemene	1FLT (VEGFA)	None	Val33, Leu54, Arg56, Leu97	Purely hydrophobic
Elemene	3ZLN (Bcl-xL)	None	Phe143, Phe144, Phe146, Met170, Leu174, Cys151	Purely hydrophobic
Elemene	4WMR (MCL-1)	None	Ile182, Ile264, Leu267/268/298, Trp312, Tyr185	Purely hydrophobic
Elemene	5DS3 (PARP-1)	None	Leu920, Ile919, Phe897, His862, Ser864, Leu877	Purely hydrophobic
Elemene	6NJS (STAT3)	None	Cys251, Ile258, Arg246, Pro256, Trp243, Lys244	Purely hydrophobic
Etoposide*	1FLT (VEGFA)	H-bond: Arg56; C–H bond: Glu30	Val33, Leu54, Pro53, Leu32	Mixed; one unfavourable Thr31 contact
Etoposide*	3ZLN (Bcl-xL)	H-bonds: Ala171, Gly148	Phe143/144/146, Ala142, Val141	Mixed; amide–π stacked
Etoposide*	4WMR (MCL-1)	H-bond: Leu186; C–H bond: Ile181	Ile287/294, Leu267/298, Val274/275	Mixed
Etoposide*	5DS3 (PARP-1)	H-bond: Gly863	Phe897, Ala898, Leu921, Val924	Mixed; π–π stacked with Phe897
Etoposide*	6NJS (STAT3)	H-bonds: Gln326, Pro255	Trp243, Lys244, Val322, Leu459	Mixed; π–π stacked with Trp243
γ-Tocopherol	1FLT (VEGFA)	π–lone-pair: Cys57	Val33, Arg56, Met78, Phe96	Weakly polar / hydrophobic

Compound	Target	Hydrogen bonds / special contacts	Dominant hydrophobic contacts	Interaction character
γ-Tocopherol	3ZLN (Bcl-xL)	None	Trp188 (π–π stacked/T-shaped), Phe143/144/146	Aromatic stacking dominant
γ-Tocopherol	4WMR (MCL-1)	H-bond: Tyr185; π-sulfur: Met199	Leu210, Ile182, Ala291, Val253	Mixed
γ-Tocopherol	5DS3 (PARP-1)	π–π: Tyr896/His862 region	Phe897, Ile990, Leu921	Mixed; unfavourable donor–donor with Tyr907
γ-Tocopherol	6NJS (STAT3)	H-bond: Gln141	Trp243, Cys251, Leu337	Sterically constrained; multiple unfavourable contacts

Integrated Candidate Prioritisation

Elemene met the threshold for all five targets with predicted affinities from −7.8 to −10.4 kcal mol^{-1}, was assigned ProTox-II Class 5, and showed one Lipinski violation and low predicted GI absorption. α-Carotene combined a four-target profile with no Lipinski violations, high predicted GI absorption, and Class 4 toxicity. Berberine and berberastine each met the threshold for four targets with no Lipinski violations and high predicted GI absorption, and both were assigned Class 3. γ-Tocopherol showed the strongest single-target affinity among the phytochemicals and met the threshold for all five proteins, but had a consensus Log P of 7.83, poor predicted aqueous solubility, and low predicted GI absorption. Ursolic acid also met the threshold for all five targets with low predicted GI absorption.

Taken together, the integrated screen identified chemically distinct candidates with different combinations of predicted target coverage, drug-likeness, absorption, and toxicity: elemene as a small five-target sesquiterpene, α-carotene as a four-target compound with favourable predicted absorption, and the structurally related isoquinoline alkaloids berberine and berberastine as four-target compounds with high predicted GI absorption. These compounds constitute a prioritised set for experimental evaluation.

DISCUSSION

This study combined molecular docking, pharmacokinetic profiling, toxicity prediction, and interaction analysis in a single multi-target screening framework applied to an ethnopharmacologically curated phytochemical library and a five-protein ovarian cancer panel. The screen produced target-, scaffold-, and pocket-specific patterns that provide a basis for ranking compounds for experimental study. Throughout the discussion that follows, docking scores are treated as predictions requiring validation; none of the interactions described has been shown experimentally in this work.

Elemene as a Multi-Target Candidate

Elemene met the threshold against all five targets, with its most favourable score against Bcl-xL (−10.4 kcal mol^{-1}). This is of interest because β-elemene, a sesquiterpene from Rhizoma zedoariae, has reported activity in ovarian cancer models: it suppresses growth and survival of both platinum-sensitive and platinum-resistant human ovarian carcinoma cells in vitro (Lee et al., 2012) and enhances cisplatin-induced apoptosis in resistant cells in association with altered BCL-2 family signalling and increased Bax expression (Li et al., 2013). The ligand docked here is the parent elemene structure retrieved from PubChem rather than the β-elemene isomer used in those studies, so the correspondence is suggestive rather than direct, and isomer-specific docking would be required before the literature could be used to support the present poses.

In the docked pose, elemene occupied the BH3-binding hydrophobic groove of Bcl-xL, contacting Phe143, Phe144, and Phe146. No hydrogen bonds were identified at any of the five interfaces; contacts were exclusively van der Waals and alkyl in character. This is chemically consistent with elemene's small, fully saturated, heteroatom-free structure and TPSA of 0 $Å^2$, and suggests that shape complementarity and hydrophobic burial, rather than directional polar contacts, underlie its predicted engagement. Such a binding mode could in principle allow accommodation within structurally diverse hydrophobic regions, which would be one explanation for its consistent scores across the panel. It is equally possible, however, that a small, flexible, purely hydrophobic ligand scores moderately well against many hydrophobic surfaces without binding specifically to any of them, since empirical scoring functions reward buried non-polar surface area. Purely hydrophobic recognition is also the interaction type least reliably modelled by rigid-receptor docking. Elemene's five-target profile should therefore be regarded as a hypothesis to be tested by direct binding assays, not as evidence of multi-target engagement.

Convergence on the Bcl-xL Hydrophobic Groove

γ-Tocopherol and elemene, despite markedly different scaffolds, both contacted the phenylalanine-rich Phe143/Phe144/Phe146 region lining the BH3-binding groove of Bcl-xL, an interface also exploited by clinically developed BH3-mimetic inhibitors. Bcl-xL and its paralogue MCL-1 were included in the panel because aberrant expression of these anti-apoptotic proteins allows ovarian cancer cells to evade

programmed cell death under therapeutic stress, a mechanism particularly relevant to platinum-resistant disease (Yan et al., 2020).

The convergence of chemically distinct ligands on this groove is consistent with recognition of a genuinely druggable region. It is, however, weak evidence on its own. The BH3-binding groove is a large, exposed hydrophobic surface and is consequently a frequent destination for docked hydrophobic ligands; convergence there is an expected outcome of the scoring function as much as a biological signal. Bcl-xL also returned the most favourable mean affinity of any target in the panel, which is consistent with this interpretation. Convergence within a docking pocket cannot establish that either compound competes with endogenous BH3-only partners, nor can it exclude scoring-function artefacts. Competition and functional assays would be required to determine whether these predicted contacts translate into modulation of Bcl-xL activity.

PARP-1 Engagement and Its Clinical Context

PARP-1 produced a distinct pattern of predicted recognition. Etoposide returned the highest predicted affinity in the dataset, −14.6 kcal mol^{-1}, forming a hydrogen bond with the backbone of Gly863 adjacent to the NAD+/nicotinamide-binding catalytic loop. This score should not be read as evidence that etoposide binds PARP-1: etoposide is a topoisomerase II poison with no established activity at PARP-1, and at 588.56 g mol^{-1} it is among the largest ligands screened, which given the observed correlation between molecular weight and docking score ($r = -0.74$) is a sufficient alternative explanation for its ranking. The result is better interpreted as an illustration of the size dependence of the scoring function than as a meaningful prediction, and it reinforces why etoposide was treated as a numerical comparator rather than a positive control.

γ-Tocopherol independently occupied the same broad sub-pocket, engaging His862 and forming π–π contacts with the Tyr896 region, together with an unfavourable donor–donor contact involving Tyr907. The presence of that unfavourable contact weakens confidence in this pose specifically.

PARP inhibitors including olaparib and niraparib have demonstrated progression-free survival benefit in ovarian cancer, although overall-survival findings contributed to the withdrawal of FDA approval for PARP inhibitor monotherapy in recurrent disease, and benefit remains concentrated in homologous-recombination-deficient subgroups (Goldlust et al., 2024). A compound able to engage PARP-1 while also interacting with Bcl-xL, MCL-1, VEGFA, and STAT3 might in principle offer broader network-level activity than a single-target agent. That proposition is speculative and is offered only as motivation for experimental work: docking cannot establish PARP-1 inhibition, simultaneous target engagement in cells, or activity independent of homologous-recombination status.

Differential Tractability of VEGFA and STAT3

The five proteins were not equally amenable to ligand docking. VEGFA returned the least favourable mean predicted affinity and STAT3 the second least favourable. The γ-tocopherol pose at STAT3 contained unfavourable steric contacts, indicating poor accommodation at that interface.

Weak performance against STAT3 is consistent with the recognised difficulty of targeting this transcription factor directly. STAT3 lacks a deep catalytic pocket of the kind presented by enzymes, and is more often addressed indirectly through upstream kinase inhibition or through its SH2 domain (Liang et al., 2020). Reduced docking performance against STAT3 should therefore be read in light of its structural characteristics rather than as evidence of low phytochemical activity. The same consideration applies to VEGFA, a largely surface-mediated protein-protein interaction target.

Some compounds nonetheless returned relatively favourable predicted STAT3 affinities, including kaempferol-7-O-rhamnoside (−8.5 kcal mol^{-1}) and 10-hydroxycamptothecin (−8.4 kcal mol^{-1}), suggesting that flavonoid glycoside and camptothecin-derived scaffolds may merit further examination for STAT3-directed activity. Natural polyphenols including resveratrol and curcumin have been reported to inhibit STAT3 phosphorylation and to reduce ovarian cancer cell motility and survival (Kim, M. J., et al., 2020; Yan et al., 2020). Docking to STAT3 does not, however, demonstrate interference with STAT3 phosphorylation, dimerisation, or transcriptional activity, and these predictions require direct validation.

Comparison with Previous Multi-Target Screening of Natural Compounds

The multi-target approach used here aligns with growing interest in applying structure-based virtual screening to natural-product libraries across several cancer-associated proteins rather than one target at a time. Sardarpour et al. (2024), for example, used a docking-based multi-target screen to identify natural compounds with potential synergistic inhibitory effects on cancer signalling pathways.

A comparable pattern emerged here: a majority of the docked library met the $\Delta G \leq -7.0$ kcal mol^{-1} threshold against at least one of the five proteins, while a much smaller group elemene, γ-tocopherol, and ursolic acid met it against all five. This separates broadly interacting candidates from compounds whose predicted activity was confined to individual proteins, and so supports prioritisation on a basis other than a single best docking score.

Ravikumar and Aittokallio (2018) have argued that appropriately selective multi-target agents may offer a better efficacy–safety balance than highly specific single-target compounds, a rationale of particular relevance to ovarian cancer, where compensatory signalling contributes to resistance (Yan et al., 2020). The present findings are compatible with that rationale but do not test it. The number of docking targets engaged is not itself evidence of superior efficacy, and whether simultaneous modulation of these five proteins would be additive, synergistic, neutral, or harmful remains an open experimental question. Broad target engagement is also the mechanism of off-target toxicity, so a high coverage score is not unambiguously favourable.

Pharmacokinetic and Toxicity Trade-Offs

Predicted binding affinity alone did not determine overall suitability. ADME and toxicity profiling revealed a clear trade-off: elemene and γ-tocopherol, among the strongest binders after the comparator, were both predicted to have low gastrointestinal absorption and poor aqueous solubility. These are recognised constraints of highly lipophilic terpenoid and tocopherol scaffolds and could limit systemic exposure irrespective of target affinity.

This pattern reflects a broader difficulty in natural-product development, in which compounds with promising in vitro or in silico activity underperform in vivo because of poor bioavailability, rapid metabolism, or inadequate tissue distribution. Formulation and derivatisation strategies, including nanoparticle encapsulation and semisynthetic modification, have been explored to address these constraints (Islam et al., 2023; Muttiah & Abdullah, 2026).

Other candidates showed a different balance. α-Carotene, berberine, and berberastine combined four-of-five target coverage with no Lipinski violations and high predicted GI absorption. Although their docking scores were lower than those of γ-tocopherol or elemene, their predicted pharmacokinetic properties may make them more tractable for oral formulation. This illustrates why ranking compounds on docking affinity alone can be misleading when pharmaceutical development is the eventual aim, and why integrating ADME assessment into the screening workflow yields information that docking scores cannot supply.

Mechanistic Plausibility in the Context of Existing Pharmacology

Several prioritised compounds have reported antitumour mechanisms in ovarian cancer models that are compatible with the proteins against which they scored comparatively well. This independent evidence does not validate the docking poses, but it provides context for assessing their plausibility.

Curcumin showed its strongest predicted affinity toward Bcl-xL (−9.4 kcal mol^{-1}), and has been reported to downregulate Bcl-xL and MCL-1 expression and promote apoptosis in cisplatin-resistant ovarian cancer cells (Yan et al., 2020), as well as to suppress fascin through the JAK/STAT3 pathway (Kim, M. J., et al., 2020). Ginsenosides scored most favourably against PARP-1 and MCL-1 here, and have reported effects on the Warburg phenotype and HIF-1α-mediated invasion involving STAT3 and ubiquitin–proteasome mechanisms (Yan et al., 2020). Berberine showed a four-of-five profile with a predicted PARP-1 affinity of −8.4 kcal mol^{-1}, and has been reported to sensitise ovarian cancer cells to PARP inhibitors by suppressing homologous recombination repair (Yan et al., 2020).

These convergences should not be read as confirmation of direct binding. In each case the reported cellular effect concerns regulation of protein expression or of signalling output, which can arise through upstream signalling, transcriptional regulation, metabolic effects, or interaction with proteins outside this panel, and is not equivalent to direct engagement of the docked protein. Direct attribution will require

biochemical or biophysical binding assays followed by functional studies able to separate primary target engagement from downstream effects.

Limitations

Several limitations qualify these results. First, AutoDock Vina scores are predictions, not measurements, and correlate imperfectly with experimental affinities. The docking protocol treated receptors as rigid and omitted water-mediated interactions and the conformational ensembles that these proteins sample in solution considerations that are especially relevant for the STAT3 SH2 domain and the conformationally variable BCL-2 family members. The search spaces used were large relative to a single site, so poses were not constrained to a validated orthosteric pocket.

Second, the screen was not validated against known actives. No re-docking of co-crystallised ligands, decoy screening, or enrichment analysis was performed, so the ability of the scoring function to discriminate binders from non-binders on this panel is unknown. The −7.0 kcal mol^{-1} threshold is an operational convenience rather than a validated cut-off, and hit counts are sensitive to its value.

Third, docking scores correlated strongly with molecular weight ($r = -0.74$), so the ranking is partly a function of ligand size. Comparisons between compounds of substantially different molecular weight are correspondingly unreliable, and ligand efficiency measures would be a more appropriate basis for cross-compound comparison in future work.

Fourth, SwissADME and ProTox-II outputs are predictive rather than experimental and cannot substitute for measured absorption, distribution, metabolism, excretion, or toxicity data (Yan et al., 2020). Where a library entry represents a class of compounds rather than a single structure, as for ginsenosides and anthocyanins, results apply only to the representative structure docked.

Fifth, etoposide was included as a numerical comparator and not as a positive control. It is a topoisomerase II poison with well-documented cumulative clinical toxicity, no established activity against any protein in this panel, and a molecular weight near the top of the screened range. Its scores neither validate the protocol nor indicate that the screened compounds share its mechanism or its toxicity profile.

Finally, much of the supporting mechanistic literature derives from two-dimensional cell culture, and few of the prioritised compounds have been evaluated in ovarian cancer xenograft models or clinical trials. These results should therefore be treated as hypothesis-generating. Biochemical or biophysical binding assays should precede target-specific functional studies in ovarian cancer cells, and candidates retaining activity would then require assessment of efficacy, pharmacokinetics, and toxicity in appropriate in vivo models before any translational claim could be supported (Efferth et al., 2017; Yan et al., 2020).

CONCLUSION

This integrated in silico screen of 45 phytochemicals against VEGFA, Bcl-xL, MCL-1, PARP-1, and STAT3 identified a small subset of compounds with favourable predicted binding across the full panel. Elemene, γ-tocopherol, and ursolic acid met the $\Delta G \leq -7.0$ kcal mol^{-1} threshold against all five targets, while α-carotene, berberine, and berberastine combined four-target coverage with more favourable predicted drug-likeness and gastrointestinal absorption. Interaction analysis distinguished three recognition patterns: elemene engaged all five proteins through hydrophobic and alkyl contacts alone, whereas γ-tocopherol and etoposide also formed hydrogen bonds and aromatic stacking contacts at the Bcl-xL BH3-binding groove and the PARP-1 catalytic loop.

Two methodological findings are worth emphasising. Incorporating pharmacokinetic and toxicity filtering into the workflow showed that the strongest docking scores did not identify the most pharmaceutically tractable compounds, and the strong correlation between docking score and molecular weight showed that affinity rankings are partly driven by ligand size. Both argue against ranking virtual screening output on binding score alone.

On this integrated basis, elemene, α-carotene, and the berberine/berberastine scaffold are the most balanced and structurally diverse candidates for follow-up. These are computational predictions and nothing more: the screen was not validated against known actives, and biochemical binding assays, cell-based functional studies, and in vivo evaluation would all be required before any conclusion could be drawn about the value of these phytochemicals as multi-target agents in ovarian cancer.

LIST OF ABBREVIATIONS

ADME, absorption, distribution, metabolism, and excretion; ADMET, absorption, distribution, metabolism, excretion, and toxicity; BBB, blood–brain barrier; Bcl-xL, B-cell lymphoma-extra large; BRCA, breast cancer susceptibility gene; CA125, cancer antigen 125; ΔG, Gibbs free energy of binding (predicted binding affinity); ESOL, estimated aqueous solubility model; FDA, U.S. Food and Drug Administration; GI, gastrointestinal; HIF-1α, hypoxia-inducible factor 1-alpha; IL-6, interleukin-6; JAK, Janus kinase; LD50, median lethal dose; Log P, logarithm of the octanol–water partition coefficient; MCL-1, myeloid cell leukemia-1; MW, molecular weight; NAD+, nicotinamide adenine dinucleotide (oxidised form); PARP-1, poly(ADP-ribose) polymerase-1; PDB, Protein Data Bank; PDBQT, Protein Data Bank, partial charge (Q), and atom type (T) format; r, Pearson correlation coefficient; P, probability value; SH2, Src homology 2 domain; SMILES, simplified molecular-input line-entry system; STAT3, signal transducer and activator of transcription 3; TPSA, topological polar surface area; USDA-ARS, United States Department of Agriculture, Agricultural Research Service; VEGFA, vascular endothelial growth factor A.

CONFLICT OF INTEREST

The author declares no conflicts of interest related to this work.

REFERENCES

Anighoro, A., Bajorath, J., & Rastelli, G. (2014). Polypharmacology: Challenges and opportunities in drug discovery. *Journal of Medicinal Chemistry, 57*(19), 7874–7887.

Armstrong, D. K., Bundy, B., Wenzel, L., Huang, H. Q., Baergen, R., Lele, S., Copeland, L. J., Walker, J. L., & Burger, R. A. (2006). Intraperitoneal cisplatin and paclitaxel in ovarian cancer. *New England Journal of Medicine, 354*(1), 34–43.

Ashworth, A., & Lord, C. J. (2018). Synthetic lethal therapies for cancer: What's next after PARP inhibitors? *Nature Reviews Clinical Oncology, 15*(9), 564–576.

Banerjee, P., Eckert, A. O., Schrey, A. K., & Preissner, R. (2018). ProTox-II: A webserver for predicting toxicity of chemicals. *Nucleic Acids Research, 46*(W1), W257–W263.

Burger, R. A., Brady, M. F., Bookman, M. A., Fleming, G. F., Monk, B. J., Huang, H., Mannel, R. S., Homesley, H. D., Fowler, J., Greer, B. E., Boente, M., Birrer, M. J., & Liang, S. X. (2011). Incorporation of bevacizumab in the primary treatment of ovarian cancer. *New England Journal of Medicine, 365*(26), 2473–2483.

Czabotar, P. E., Lessene, G., Strasser, A., & Adams, J. M. (2014). Control of apoptosis by the BCL-2 protein family: Implications for physiology and therapy. *Nature Reviews Molecular Cell Biology, 15*(1), 49–63.

Daina, A., Michielin, O., & Zoete, V. (2017). SwissADME: A free web tool to evaluate pharmacokinetics, drug-likeness and medicinal chemistry friendliness of small molecules. *Scientific Reports, 7*, Article 42717.

Duke, J. A. (n.d.). *Dr. Duke's Phytochemical and Ethnobotanical Databases*. United States Department of Agriculture, Agricultural Research Service. https://phytochem.nal.usda.gov/

Efferth, T., Saeed, M. E. M., Mirghani, E., Alim, A., Yassin, Z., Saeed, E., Khalid, H. E., & Daak, S. (2017). Integration of phytochemicals and phytotherapy into cancer precision medicine. *Oncotarget, 8*(30), 50284–50304.

Ferlay, J., Colombet, M., Soerjomataram, I., Parkin, D. M., Piñeros, M., Znaor, A., & Bray, F. (2024). Global cancer statistics 2022: GLOBOCAN estimates of incidence and mortality worldwide for 34 cancers in 186 countries. *CA: A Cancer Journal for Clinicians*. https://doi.org/10.3322/caac.70090

Goldlust, I. S., Guidice, E., & Lee, J. (2024). PARP inhibitors in ovarian cancer. *Seminars in Oncology, 51*(1–2), 45–57.

Islam, M. R., Rahman, M. M., Dhar, P. S., Nowrin, F. T., Sultana, N., Akter, M., Rauf, A., Khalil, A. A., Gianoncelli, A., & Ribaudo, G. (2023). The role of natural and semi-synthetic compounds in ovarian cancer: Updates on mechanisms of action, current trends and perspectives. *Molecules, 28*(5), Article 2070.

Jha, V., Devkar, S., Gharat, K., Kasbe, S., Matharoo, D. K., Pendse, S., Bhosale, A., & Bhargava, A. (2022a). Screening of phytochemicals as potential inhibitors of breast cancer using structure based multitargeted molecular docking analysis. *Phytomedicine Plus, 2*, Article 100227.

Jha, V., Bhosale, A., Kapadia, P., Bhargava, A., Marick, A., Charania, Z., Parulekar, O., Shaikh, M., & Madaye, B. (2022b). Multitargeted molecular docking study of phytochemicals on hepatocellular carcinoma. *Journal of Applied Biology & Biotechnology*.

Johnson, D. E., O'Keefe, R. A., & Grandis, J. R. (2018). Targeting the IL-6/JAK/STAT3 signalling axis in cancer. *Nature Reviews Clinical Oncology, 15*(4), 234–248.

Kim, M. J., Park, K.-S., Kim, K.-T., & Gil, E. Y. (2020). The inhibitory effect of curcumin via fascin suppression through JAK/STAT3 pathway on metastasis and recurrence of ovary cancer cells. *BMC Women's Health, 20*, Article 256.

Kim, S., Chen, J., Cheng, T., Gindulyte, A., He, J., He, S., Li, Q., Shoemaker, B. A., Thiessen, P. A., Yu, B., Zaslavsky, L., Zhang, J., & Bolton, E. E. (2023). PubChem 2023 update. *Nucleic Acids Research, 51*(D1), D1373–D1380.

Lee, R. X., Li, Q. Q., & Reed, E. (2012). β-Elemene effectively suppresses the growth and survival of both platinum-sensitive and -resistant ovarian tumor cells. *Anticancer Research, 32*(8), 3103–3113.

Li, Q. Q., Lee, R. X., Liang, H., Zhong, Y., & Reed, E. (2013). Enhancement of cisplatin-induced apoptosis by β-elemene in resistant human ovarian cancer cells. *Medical Oncology, 30*(1), Article 424.

Liang, R., Chen, X., Chen, L., Wan, F., Chen, K., Sun, Y., & Zhu, X. (2020). STAT3 signaling in ovarian cancer: A potential therapeutic target. *Journal of Cancer, 11*(4), 837–848.

Moore, K., Colombo, N., Scambia, G., Kim, B.-G., Oaknin, A., Friedlander, M., Lisyanskaya, A., Floquet, A., Leary, A., Sonke, G. S., Gourley, C., Banerjee, S., Oza, A., González-Martín, A., Aghajanian, C., Bradley, W., Mathews, C., Liu, J., Lowe, E. S., ... DiSilvestro, P. (2018). Maintenance olaparib in patients with newly diagnosed advanced ovarian cancer. *New England Journal of Medicine, 379*(26), 2495–2505.

Muttiah, B., & Abdullah, N. A. H. (2026). Natural compounds in ovarian cancer: Mechanistic insights and therapeutic potential. *Frontiers in Pharmacology, 16*, Article 1687805.

Newman, D. J., & Cragg, G. M. (2020). Natural products as sources of new drugs over the nearly four decades from 01/1981 to 09/2019. *Journal of Natural Products, 83*(3), 770–803.

Ravikumar, B., & Aittokallio, T. (2018). Improving the efficacy-safety balance of polypharmacology in multi-target drug discovery. *Expert Opinion on Drug Discovery, 13*(2), 179–192.

Sardarpour, N., Goodarzi, Z., & Gharaghani, S. (2024). Docking-based virtual screening method for selecting natural compounds with synergistic inhibitory effects against cancer signalling pathways using a multi-target approach. *Iranian Journal of Biotechnology, 22*(2), Article e3718.

Sung, H., Ferlay, J., Siegel, R. L., Laversanne, M., Soerjomataram, I., Jemal, A., & Bray, F. (2021). Global cancer statistics 2020: GLOBOCAN estimates of incidence and mortality worldwide for 36 cancers in 185 countries. *CA: A Cancer Journal for Clinicians, 71*(3), 209–249.

Trott, O., & Olson, A. J. (2010). AutoDock Vina: Improving the speed and accuracy of docking with a new scoring function, efficient optimization, and multithreading. *Journal of Computational Chemistry, 31*(2), 455–461.

Yan, Y.-B., Tian, Q., Zhang, J.-F., & Xiang, Y. (2020). Antitumor effects and molecular mechanisms of action of natural products in ovarian cancer [Review]. *Oncology Letters, 20*(5), Article 141.